

# A Cost-effective RISs Deployment to abate the Coverage Problem in B5G Networks

Guillermo Encinas-Lago, *Student Member, IEEE*, Antonio Albanese, *Member, IEEE*,  
Vincenzo Sciancalepore, *Senior Member, IEEE*, Xavier Costa-Pérez, *Senior Member, IEEE*,  
Albert Banchs, *Senior Member, IEEE*, Dinh-Thuy Phan-Huy, *Member, IEEE*

**Abstract**—As upcoming, beyond-5G (B5G) wireless network generations are expected to deliver much better performance than existing solutions, Reconfigurable intelligent surfaces (RISs) are gaining relevance as one of the new key technologies able to facilitate such improvement. Interestingly, they can redesign how the propagation environment is conceived by giving an opportunity to programmatically alter it: they can be configured to behave as orientable mirrors, scatterers, or lenses. This flexibility allows for the successful exploitation of bands which provide superior performance in wireless links but present poor propagation properties.

However, this fascinating technology comes at not negligible costs: RISs require ad-hoc design, deployment and management operations to be fully exploited. In this paper, we tackle one of the open problems in the RISs literature: the optimal placement. We propose a model-based and a model-free approach, respectively RISA and AI-RISA, showcasing their large-scale solutions on synthetic topologies to improve communication performance while solving the “dead-zone” coverage problem. Additionally, our frameworks are empirically validated within a realistic indoor scenario, the Rennes railway station, showing how a complex indoor propagation environment can be fully disciplined by an advanced RISs installation.

## I. INTRODUCTION

Lately, the new generation of cellular networks has been successfully integrated and deployed bringing along new business opportunities. However, the revenue-hungry telco operators continuously look for innovative solutions to enable novel use cases, which involve new players into the engaged business model. Within this context, one emerging technology aims at undermining the classical communication paradigm—that dogmatized the radio propagation environment as an ungovernable box—providing new means to exploit the signal properties: *reconfigurable intelligent surfaces (RISs)* [1]. Agility and flexibility represent a compelling added-value for this solution [2]: while RISs can be dynamically and

continuously configured, they draw little power with affordable installation and maintenance costs [3]. Manufactured as passive arrays of reflective elements able to backscatter and phase-shift the radio frequency (RF) power incident onto their surface, they are expected to be soon inexpensive enough to be massively deployed on building walls, similarly to, e.g., conventional wallpapers [4]. Besides, although currently available RISs prototype rely on a dedicated control channel to operate, the advancement of self-configuring RISs within the novel Internet-of-Surfaces (IoS) paradigm commits to relax their dependency on external control, thus further facilitating their deployment in the view of plug-and-play RISs that can be seamlessly integrated in the current network infrastructure without disruption [5].

Such a technology may come into the picture when tackling the mobile dead-zone problem in indoor scenarios by enabling very-dense RIS-based network deployment at low Capital Expenditure (CAPEX). Ubiquitous high quality coverage is one of the main pillars of the upcoming sixth generation (6G) cellular network, being it pivotal for innovative use cases such as round-the-clock remote healthcare management, immersive extended reality, or Industry X.0 [6]. However, as shown in Fig. 1 for the case of a real railway station, the existing network infrastructure may fail to guarantee satisfactory performance within the entire environment: *How to solve the dead-zone problem with a limited investment?* RIS are being explored in the literature as a potential answer, thanks to their low manufacturing cost and minimal energy consumption: as long as installation and licensing costs do not dominate—considering they are lightweight, radio-wise passive devices—, the investment required to employ RISs will be negligible in comparison to full fledged traditional base stations (BSs). Developing ad-hoc RIS design and deployment strategies might be the correct approach, though at the expense of additional complexity. Indeed, while RISs properly steer the reflect beams towards specific directions, interference is also focused onto unwanted areas, if not properly manipulated [7]. This issue exacerbates the overall deployment intricacy calling for advanced optimization techniques to strike the optimal trade-off between RISs density and the corresponding spurious detrimental interference.

Traditionally, this problem has been addressed by the generic BSs deployment problem, which is a fundamental issue for cellular networks and has been extensively investigated in the literature [8]. Nonetheless, the vast majority of the available research works assume isotropic radiating

Guillermo Encinas-Lago is with NEC Laboratories Europe, 69115 Heidelberg, Germany and Université Paris-Saclay, CNRS, CentraleSupélec, Laboratoire des Signaux et Systèmes, 91190 Gif-sur-Yvette, France.

Antonio Albanese is with Flyhound Co., 10019, New York, USA, and Universidad Carlos III of Madrid, 28911 Leganés, Spain.

Vincenzo Sciancalepore is with NEC Laboratories Europe.

Xavier Costa-Pérez is with i2cat, ICREA, 08034 Barcelona, Spain and NEC Laboratories Europe.

Albert Banchs is with University Carlos III of Madrid and IMDEA Networks Institute, 28911 Leganés, Spain.

Dinh-Thuy Phan-Huy is with Radio InnOvation (RIO) Department, Orange Innovation (INNOV), 92320 Chatillon, France.

Email of the corresponding author: Guillermo.Encinas@neclab.eu.

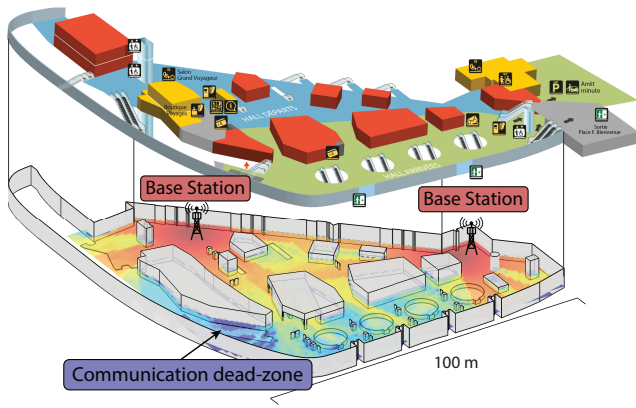


Fig. 1: Railway station topographic map and related power heatmap showing the dead-zone problem (Rennes, France).

antennas, which make the problem easy-to-tackle by means of graph-coloring algorithms or convex programming approaches. When dealing with directive transmissions—e.g., millimeter waves (mmWaves) above 6 GHz—a new degree of freedom is introduced: the beam orientation. Specifically, mmWave BSs must be properly placed and electronically oriented to effectively beam towards specific locations leveraging on the available channel state information (CSI) [9].

In this context, an ideal RISs deployment is even harder to achieve: on the one hand, the optimal RISs deployment requires a priori information on the applied RISs configurations, on the other hand, the optimal RISs configurations can be obtained only upon fixing the BSs and RISs positions as well as the BSs-user equipments (UEs) associations. To overcome this issue and make the analysis tractable, previous efforts in the literature rely on simplistic assumptions on agnostic RISs optimization [10]. Differently, in this paper, we go one step beyond and jointly tackle the optimal RISs placement problem and RISs configuration without any unpractical assumption on the availability of instantaneous CSI or high-speed re-configuration capabilities of the RIS. Besides, we tackle the problem in its multi-user form to prevent oversimplifying single-user solutions, that could not be adapted to realistic network conditions.

To this aim, we design the following two alternative techniques. The first approach relies on the well-known Block Coordinate Ascent (BCA) [11] to devise RISA, a RIS-Aware network planning solution that iteratively triggers RISs configurations and optimally places the required number of RISs within the area. Building upon a *model-based* formulation, RISA assumes line-of-sight (LoS) wireless links, which allow characterizing the network only based on its geometry without detailed RF propagation modeling. The second approach, dubbed as Artificial Intelligence (AI)-RISA, consists of a reinforcement learning (RL)-based technique that takes advantage of ad-hoc ray tracing simulations to optimally tailor the RISs deployment and configurations to the features of the propagation environment. Such novel *model-free* data-driven solution removes the LoS assumption, which could lead to performance losses in particularly challenged propagation scenarios, at the expense of higher complexity due to extensive

3D mapping of the environment. The use of ray tracing simulations to evaluate the deployments obtained by RISA and to fully drive the solution production process with AI-RISA ensures that we take into account both scatterers and fading phenomena present in the environment, despite our initial assumption of LoS between candidate sites (CSs) and both BSs and UEs.

As main contributions, we *i*) create a new ray-tracing (RT) model, able to simulate multi-RIS situations, *ii*) develop RISA, an iterative algorithm based on Block Coordinate Descent to solve the deployment problem, *iii*) prove, both analytically and empirically, the ability of RISA of converging in a short time, *iv*) improve the capability of RISA against environments with complex propagation properties conceiving AI-RISA, a data-driven solution, based on RL techniques guided by the results of the ad-hoc ray tracing computations, *v*) examine the efficiency of both RISA and AI-RISA in large-scale scenarios, *vi*) exhibit the behaviour of both in a realistic simulation of the Rennes Train Station in France, revealing their outstanding performance and illustrating how these algorithms can improve the cellular infrastructure currently deployed by one of the major European operators, fixing the dead-zone problem, and *vii*) verify the efficacy of our proposals comparing them against exhaustive search (ES) and the current state-of-the-art solutions in the performance benchmark.

The remainder of this paper is as follows. Section II includes a survey of the related literature, followed by Section III-A which introduces the system model, while Section III-B presents the multi-RIS coverage enhancement problem and discusses its analytical tractability. In Section IV, we tackle the aforementioned problem and derive a more tractable relaxation, i.e. the Multi-RIS planning problem, which we iteratively solve in Section IV-B by means of the proposed RISA. AI-RISA is illustrated in Section V while both approaches are numerically validated by simulations against state-of-the-art (SOA) and heuristic solutions in Section VI, wherein we also illustrate our RT model for multi-RIS scenarios. Finally Section VII concludes the paper.

## NOTATION

We denote matrices and vectors in bold while each of their element is indicated in roman with a subscript. Operation  $(\cdot)^T$  represents the vector or matrix transposition,  $\otimes$  stands for the Kronecker product while  $(\cdot)^H$  denotes the Hermitian transposition. The L2-norm of a vector is written as  $\|\cdot\|$ .  $\mathbb{R}$  and  $\mathbb{R}^+$  indicate the sets of real and positive real numbers, respectively, while  $\mathbb{C}$  is the set of complex numbers.

## II. RELATED WORK

**RF planning.** Planning the BS deployment is key to the effectiveness of any cellular network and is therefore one of the oldest problems in modern wireless communications [12]. Typically, literature works aim at optimizing the coverage probability [8], [13], [14], although the latter is shown to be almost invariant with respect to the network geometry in case of massive deployments [15]. Such Key Performance Indicator (KPI) is more often than not insufficient to assess the

performance of more recent radio access networks [16]–[18]. Indeed, the advent of 5G-and-beyond-5G (B5G) millimeter-wave (mm-Wave) technology has brought up a series of new deployment challenges [19], namely reliability under blockage [20], fast cell discovery [21] or ultra-dense non-uniform deployments [22], [23], which call for novel heuristic algorithms or machine learning (ML) approaches [24]–[28], in order to optimize, e.g., coverage, throughput, reliability, UEs mobility, latency. Differently from the above-mentioned works, in this paper we consider the problem of RIS-aided network deployment, which is still an open research topic to be tackled before commercial RISs deployment

**Smart radio environment (SRE).** RISs are drawing increasingly higher interest from the research community and the industry as a new disruptive technology enabling the transition to 6G cellular networks [29]–[31]. Indeed, RISs will be pivotal for innovative use cases, such as immersive virtual reality, high-fidelity holographic projections, digital twins, electromagnetic exposure isolation, and first-responders operations assistance, which are not readily supported by existing networks [6], [32]. Furthermore, integrating RISs in the current network infrastructure represents a cost-effective and power-efficient alternative to an ultra-dense deployment of fully-fledged BSs when it comes to mitigating the sensitivity to blockages and the severe pathloss typical of mm-Wave communications [33], [34]. The relevance of RIS in narrow-band and wide-band applications has been discussed in works as [35], [36].

**RISs optimization.** The vast majority of literature items about SRE tackles the problem of optimally configuring RISs as to maximize several KPIs [37], [38]. In particular, [39] shows that RIS-aided networks achieve throughput similar to legacy massive multiple-input multiple-output (MIMO) systems using fewer active elements when joint active (at the BSs) passive (at the RISs) beamforming is performed. The square power gain against the number of reflective elements holds even with quantized phase shifts at the RISs elements, net of some additional power loss that depends on the number of available quantization levels [40]. Recent optimization approaches leverage on statistical CSI to reduce the overhead on the feedback channel necessary to propagate instantaneous CSI [41], e.g. by maximizing the average sum-rate under a general correlated Rician channel model [42] or by assuming prior statistical characterization of the UEs locations [43], [44], or explore the effect of different degrees of CSI availability [45]. In this regard, the novel concept of IoS has opened up the possibility of employing self-configuring smart surfaces, which suffer from limited performance degradation with respect to managed RISs deployments that rely on dedicated control channels, and require little modifications to the conventional RIS hardware design [5]. Despite the high research interest around RISs and SRE, the RF planning problem of RISs-aided cellular networks is almost untouched [10].

**ML-assisted wireless communications.** ML approaches have proved to be effective for a variety of communications-related problems [46], [47]. Older works such as [48] use supervised learning on Support Vector Machines (SVMs)

to select the optimal MIMO antenna indices, showing high resilience against transceivers non-linearities. However, more recent applications often leverage on the wide-spread Neural Networks (NNs), achieving high accuracy at the expense of model explainability. NNs are often used to approximate objective functions for link budget and propagation loss for next-generation wireless networks [49], as mapping functions between the propagation environment and the MIMO beamforming vectors [50], or to perform channel estimation [45]. Equally common are RL approaches because of the stochastic operational conditions of wireless networks, which need to counteract numerous environmental uncertainties. In this regard, an agent can learn from experience and obtain the optimal decision policy by trial and error [51]. For instance, the Deep Reinforcement Learning solution in [52] overcomes the limitations of pre-defined beamforming codebooks in mm-Wave networks by learning beam patterns so as to adapt to the propagation environment, including the user distribution, array geometry, and possible hardware impairments. When it comes to pure RL approaches, a vast portion of the literature leverages on Q-learning. Its applications span over several topics, including opportunistic channel access [53], adaptive sleep-scheduling algorithms for wireless nodes [54], handover optimization in heterogeneous networks [55], and so forth. As reference, [56] employs Q-learning to design trajectory, the phase shifts, the power allocation policy of a RIS mounted on an unmanned aerial vehicle, achieving significant flight and transmission energy saving.

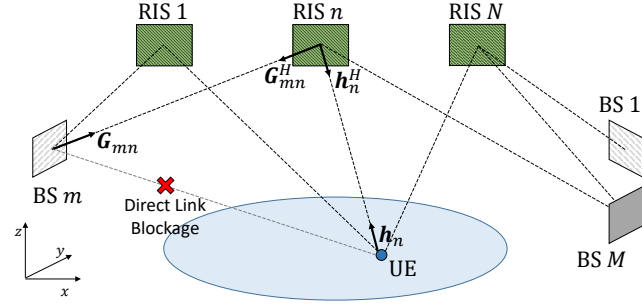
### III. MODEL DESIGN

Let us first focus our attention on our model-based approach, i.e. RISA<sup>1</sup>, and lay its foundation by introducing the reference system model as well as the mathematical formulation of the multi-RIS coverage problem.

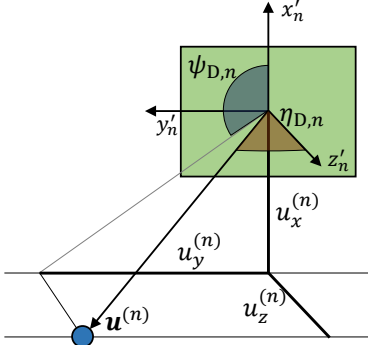
#### A. System Model

We consider the RIS-enabled wireless network depicted in Fig. 2(a), wherein  $N$  RISs are deployed to assist  $M$  BSs to extend their communication coverage in a given area of interest  $\mathcal{A}$ . Please note that our model is explicitly multi-user, although Fig. 2 depicts a single user for the sake of clarity. We model each BS as a uniform linear array with  $N_b$  antennas, and each RIS as a planar linear array with  $N_r = N_h \times N_v$  reflective elements, where  $N_h$  and  $N_v$  denote the number of elements in the horizontal plane and the vertical direction of the absolute reference system, respectively. We indicate by  $\mathbf{b}_m \in \mathbb{R}^3$ ,  $\mathbf{r}_n \in \mathbb{R}^3$  and  $\mathbf{u} \in \mathbb{R}^3$  the locations of the  $m$ -th BS center, the  $n$ -th RIS center and the typical UE, respectively. We assume that the direct LoS links from the BSs provide negligible received power in the target area due to blockage or severe shadowing. Therefore, the communication between BSs and UEs must be carried out over the reflected links through the RISs. We would like to point out that the simultaneous assumptions of LoS between the RISs and both BSs and UEs, and blockage of the links between the BSs

<sup>1</sup>Our model-free approach, AI-RISA, is introduced in Section V.



(a) Reference network deployment including BSs, RISs and one sample UE.



(b) Sample user equipment (UE) detail in the  $n$ -th RIS reference system.

Fig. 2: Geometrical aspects of the considered scenario. Multiple users omitted for clarity.

and the UEs are not contradictory. Indeed, we focus our work on areas without coverage for traditional BSs deployments, hence the blockage between the BSs and the UEs, and choose deployment locations for the RISs that are in LoS of the BSs and the UEs. We later confirm the LoS and the blockage assumptions in the considered realistic scenario by means of RT simulations. While the use of the RT provides us the necessary information about the connections between transmitter, RIS and receiver, there are circumstances where this technique is unavailable or imprecise for channel estimation. In those cases a proper study of the downlink and uplink characteristics becomes fundamental, as in [57]. This study needs to take into account not only the fading model, but also the multiple access method. All these parameters impact the communications and can lead to different optimal deployments, hence their importance. In the present work, we assume that each BS can leverage on multiple RISs but each RIS is used and controlled by a single BS, which connects to the on-board RIS controller via a separate (wired or wireless) reliable control link. Moreover, we consider a flat-fading<sup>2</sup> channel over which multi-UE communication is achieved by means of orthogonal frequency-division multiple access (OFDMA) [57], [58]. We will further discuss the network resource allocation later in Section IV-A. Focusing on the downlink transmission, the  $m$ -th BS transmits data to the UE over the reflected links through the  $n$ -th RIS. Such path can be decomposed into the LoS channel  $\mathbf{h}_n \in \mathbb{C}^{N_r \times 1}$  between the RIS and the UE, and

the LoS channel  $\mathbf{G}_{mn} \in \mathbb{C}^{N_r \times N_b}$  between the BS and the RIS.

Let us indicate as  $\Lambda_m$ , with cardinality  $|\Lambda_m|$ , the set of RISs that are associated with BS  $m$ . The received downlink signal at the UE is given by the superposition of the signals incoming from all BSs through their associated RISs, namely

$$y \triangleq \sum_{m=0}^{M-1} \sum_{n=0}^{|\Lambda_m|} (\mathbf{h}_n^H \Phi_n \mathbf{G}_{mn}) \mathbf{w}_m s + n \in \mathbb{C}, \quad (1)$$

where  $\Phi_n = \text{diag}[\alpha_{n1}e^{j\phi_{n1}}, \dots, \alpha_{nN}e^{j\phi_{nN}}]$  with  $\phi_{ni} \in [0, 2\pi]$  and  $|\alpha_{ni}|^2 \leq 1$ ,  $\forall i$  indicate the phase shifts and amplitude attenuation introduced by the  $n$ -th RIS,  $\mathbf{w}_m \in \mathbb{C}^{N_b \times 1}$  is the transmit precoder at the  $m$ -th BS while  $s \in \mathbb{C}$  is the transmit signal with  $|s|^2 = 1$ , and  $n \in \mathbb{C}$  is the additive white Gaussian noise term distributed as  $\mathcal{CN}(0, \sigma^2)$ .

As 3rd Generation Partnership Project (3GPP) cellular standards require the UE to be served by a single BS, we remark that the UE receives useful signal only from one BS, e.g., the  $m$ -th BS, and suffers from the interference produced by all other BSs. Therefore, the received signal-to-interference-plus-noise ratio (SINR) at the UE can be written as

$$\text{SINR}(\mathbf{u}) \triangleq \frac{\left| \sum_{n=0}^{|\Lambda_m|} (\mathbf{h}_n^H \Phi_n \mathbf{G}_{mn}) \mathbf{w}_m \right|^2}{\sum_{\substack{l=0, \\ l \neq m}}^{M-1} \left| \sum_{n=0}^{|\Lambda_l|} (\mathbf{h}_n^H \Phi_n \mathbf{G}_{ln}) \mathbf{w}_l \right|^2 + \sigma^2}, \quad (2)$$

where we observe that the BSs-RISs and RISs-UE channels are completely defined (coherently with our assumptions) by the geometry of the deployment and the user distribution. The RISs and BSs configurations, in the form of the phase shifts and precoders applied to their antenna arrays, depend both on those distributions but also on the BSs-RISs and BSs-UE associations.

In order to write the channels  $\mathbf{h}_n$  and  $\mathbf{G}_{mn}$ , we first consider  $N$  reference systems with origin in the center of each RIS and the  $(x', y')$ -plane lying on the RIS surface, as shown in Fig. 2(b). Hence, the coordinates of the UE in the reference system of the  $n$ -th RIS can be obtained as  $\mathbf{u}^{(n)} = \mathbf{R}_n \mathbf{u}$ , where

$$\mathbf{R}_n \triangleq (\hat{\mathbf{r}}_{n,x'}, \hat{\mathbf{r}}_{n,y'}, \hat{\mathbf{r}}_{n,z'}) \in \mathbb{R}^{3 \times 3}, \quad (3)$$

with  $\hat{\mathbf{r}}_{n,x'}$ ,  $\hat{\mathbf{r}}_{n,y'}$  and  $\hat{\mathbf{r}}_{n,z'} \in \mathbb{R}^3$  representing the coordinates of the  $n$ -th RIS reference system axes in the absolute reference system. Furthermore, we denote by  $\psi_{D,n}$  and  $\eta_{D,n}$  the azimuth and the zenith angle of departure (AoD) for the communication link from the RIS to the UE. Therefore, the RIS array response vector is given by

$$\mathbf{b}_{T,n}(\mathbf{u}) \triangleq \mathbf{b}_y(\psi_{D,n}, \eta_{D,n}) \otimes \mathbf{b}_z(\psi_{D,n}, \eta_{D,n}) \in \mathbb{C}^{N_r \times 1} \quad (4)$$

$$= [1, e^{j2\pi\delta \sin(\psi_{D,n}) \sin(\eta_{D,n})}, \dots, e^{j2\pi\delta(N_y-1) \sin(\psi_{D,n}) \sin(\eta_{D,n})}]^T \\ \otimes [1, e^{j2\pi\delta \cos(\psi_{D,n}) \sin(\eta_{D,n})}, \dots, e^{j2\pi\delta(N_x-1) \cos(\psi_{D,n}) \sin(\eta_{D,n})}]^T, \quad (5)$$

where  $\delta$  indicates the antenna spacing-wavelength ratio. We refer to  $\Omega_{T,n}(\mathbf{u}) \triangleq \cos(\psi_{D,n}) \sin(\eta_{D,n}) = \frac{u_x^{(n)}}{\|\mathbf{u}^{(n)}\|}$  and  $\Psi_{T,n}(\mathbf{u}) \triangleq$

<sup>2</sup>The flat fading assumption used in RIS is common for RIS related operations, but it may not hold in wideband systems. In this case, AI-RIS shows much better suitability.

$\sin(\psi_{D,n})\sin(\eta_{D,n}) = \frac{u_y^{(n)}}{\|\mathbf{u}^{(n)}\|}$  as the spatial frequencies along the  $x'_n$  and the  $y'_n$ -axis corresponding to the AoD towards the UE at absolute coordinates  $\mathbf{u}$ . Therefore, the LoS  $n$ -th RIS-UE channel is given by

$$\mathbf{h}_n(\mathbf{u}) \triangleq \sqrt{\gamma_n(\mathbf{u})} \mathbf{b}_{T,n}(\mathbf{u}) \in \mathbb{C}^{N_r \times 1}, \quad (6)$$

where  $\gamma_n(\mathbf{u}) \triangleq d_n(\mathbf{u})^{-\beta}$  is the channel power gain with  $d_n(\mathbf{u}) = \|\mathbf{r}_n - \mathbf{u}\|$  the Euclidean distance between the RIS and the UE. We would like to point out that we neglect the frequency dependency of the channel power gain due to the flat-fading nature of the channel<sup>3</sup>. In a similar way, the LoS channel between the  $m$ -th BS and the  $n$ -th RIS can be written as

$$\mathbf{G}_{mn} \triangleq \sqrt{\gamma_{Gmn}} \mathbf{b}_{R,n}(\mathbf{b}_m) \mathbf{a}_m^H(\mathbf{r}_n) \in \mathbb{C}^{N_r \times N_b}, \quad (7)$$

where  $\gamma_{Gmn} \triangleq d_{mn}^{-\beta}$  is the channel power gain with  $d_{mn} = \|\mathbf{b}_m - \mathbf{r}_n\|$ ,  $\mathbf{a}_{R,n}(\mathbf{b}_m)$  is the array response vector at the RIS corresponding to the angle of arrival from BS  $m$ , which is derived analogously to Eq. (4), and  $\mathbf{a}_m(\mathbf{r}_n)$  indicates the BS array response, defined as

$$\mathbf{a}_m(\mathbf{r}_n) \triangleq [1, \dots, e^{j2\pi\delta(M-1)\cos(\theta_{D,mn})}]^T \in \mathbb{C}^{N_b \times 1}, \quad (8)$$

where  $\theta_{D,mn}$  represents the AoD from the  $m$ -th BS to the  $n$ -th RIS. Eqs. (6), (7) neglect non-line-of-sight (NLoS) paths. This LoS assumption is corroborated by the fact that RISs are typically operated at millimeter-wave frequencies, whose higher attenuation makes the LoS paths dominant over the others.

### B. Problem Formulation

**Analytical tractability.** The solution to our planning problem requires determining the optimal RIS deployment to provide coverage within the target area, e.g., by maximizing the worst-case received SINR at all locations  $\mathbf{u}$ . To achieve this, we need to simultaneously obtain the active transmission beamformers of the BSs, and, for each RIS, their deployment location, their passive beamforming configuration, and their associated BSs, which in turn affect the optimal associations between BSs and UEs. This problem is highly non-convex and difficult to approach, owing to the inextricable entanglement between its parts. We are not able to solve the BSs-RISs association, the BSs-UEs associations, or the configurations of the different network elements without taking into account the mutual dependencies between them. For instance, even for a reduced scenario (much simpler than the one we consider) including only one BS and one RIS and given BS-RIS-UEs associations, jointly optimizing the beamforming at the BS and the RIS to cover multiple UEs locations does not yield a closed-form formulation but rather requires tackling a non-convex problem by alternatively solving the two separate beamforming optimizations until convergence [39].

Therefore, for the sake of analytical tractability, we only consider one-RIS path and a cellular-like architecture in which each RIS provides coverage to one contiguous subarea, thus

reducing the scope of the interference generated by the remaining RISs to the sole overlapping area edges. We would like to highlight that at planning stage, the RISs beamforming design for area coverage enhancement cannot take advantage of the knowledge of the instantaneous CSI of any particular UE in the area. Hence, although RISs controlled by the same BS can be configured to cover the same subarea, it is highly complex to enforce in-phase constructive interference of signals incoming from different RISs even if transmitted by the same BS.

Let us consider the UE to be inside the subarea served by BS  $m$  through RIS  $n$ . In these conditions, its received SINR can be then approximated by its signal-to-noise ratio (SNR), which is defined as

$$\text{SNR}(\Phi_n, \mathbf{w}_m, \mathbf{u}) \triangleq \frac{|\mathbf{h}_n^H \Phi_n \mathbf{G}_{mn} \mathbf{w}_m|^2}{\sigma^2}, \quad (9)$$

where  $\Phi_n$  and  $\mathbf{w}_m$  need to be optimized.

**Optimization variables.** We assume that the RISs are deployed only at specific locations, namely CSs to reflect the fact that network operators are required to meet logistical, administrative and physical constraints in real-life scenarios. Nonetheless, in the absence of CSs, our multi-RIS planning may be likewise executed by considering any sampling of the deployment area. We denote the CSs set as  $\{\mathbf{b}_m\}_{m=1}^M$ , namely the pre-defined candidate RISs coordinates (position and orientation), and we take care of selecting at which of them RISs are actually deployed. The specific locations of these CSs, namely the input to our algorithm, follow feasibility criteria in terms of architectural and installation constraints. In addition, they need to comply with the LoS requirement with the BSs and the UEs. Besides, we sample the target area by means of  $T$  test points (TPs)  $\mathbf{u}_t \in \mathcal{A}$ , wherein we optimize the SNR of the typical UE<sup>4</sup>. Our planning solution outputs the set of RISs to be deployed while providing the optimal BS-RIS-UE association at each test point. We thus introduce decision variables  $\mathbf{x} \in \{0, 1\}^N$  and  $\mathbf{y} \in \{0, 1\}^{T \times M \times N}$ , whose elements  $x_n$  and  $y_{tmn}$  indicate whether a RIS is deployed at CS  $n$ , and the association between the typical UE at TP  $\mathbf{u}_t$ , BS  $m$  and RIS at CS  $n$ , respectively.

**RISs planning.** We can now formulate the multi-RIS coverage enhancement problem as the following

<sup>3</sup>This simplification does not affect the problem formulation nor its algorithmic solutions RISA and AI-RISA.

<sup>4</sup>Ideally, the TP distribution should match the expected distribution of the users in the target area but the problem formulation remains valid for any distribution of users.

*Problem 1 (Multi-RIS coverage enhancement):*

$$\max_{\Phi_n, \mathbf{w}_m, \mathbf{x}, \mathbf{y}} \min_{\mathbf{u}_t \in \mathcal{A}} \sum_{m,n} y_{tmn} |\mathbf{h}_n^H \Phi_n \mathbf{G}_{mn} \mathbf{w}_m|^2 \quad (10a)$$

$$\text{s.t. } |\Phi_{n,ii}|^2 \leq 1, \quad \forall n, \forall i, \quad (10b)$$

$$\|\mathbf{w}_m\|^2 \leq P, \quad \forall m, \quad (10c)$$

$$y_{tmn} \hat{\mathbf{r}}_{n,x'}^T (\mathbf{u}_t - \mathbf{r}_n) \geq 0, \quad \forall t, \forall m, \forall n, \quad (10d)$$

$$y_{tmn} \hat{\mathbf{r}}_{n,x'}^T (\mathbf{b}_m - \mathbf{r}_n) \geq 0, \quad \forall t, \forall m, \forall n, \quad (10e)$$

$$y_{tmn} \leq x_n, \quad \forall t, \forall m, \forall n, \quad (10f)$$

$$\sum_{m,n} y_{tmn} = 1, \quad \forall t, \quad (10g)$$

$$\sum_m \max_t y_{tmn} \leq 1, \quad \forall n \quad (10h)$$

$$\sum_n x_n = L, \quad (10i)$$

$$x_n \in [0, 1], \quad y_{tmn} \in [0, 1], \quad \forall t, \forall m, \forall n, \quad (10j)$$

where we omit the constant noise term  $\sigma^2$  and refer to the available transmit power at the BSs as  $P$ . The constraints in Eq. (10b) and Eq. (10c) cover the energy consumption limits of the involved devices. We consider only fully passive RISs, hence the inequality on Eq. (10b), and we set a homogeneous power limit across BSs by limiting each precoder  $\mathbf{w}_m$  with the constraint in Eq. (10c). Constraints (10d) and (10e) guarantee that each RIS can respectively serve a TP or be assigned to a BS only if they front the RIS, i.e. only if the vector originated in the RIS and pointing towards the TP or the BS has a positive projection on the RIS orientation vector  $\hat{\mathbf{r}}_{n,x'}$ . Moreover, constraint (10f) states that a RIS should be deployed only if at least the UE located at one TP would exploit it, whereas constraint (10g) reflects the fact that each TP must be covered by only one RIS. Constraint (10h) forces each CS to be associated to at most one BS and, lastly, we enforce the number of deployed RISs to be equal to  $L$  in constraint (10i), where  $L$  is the number of RISs to be deployed by the network operator. Please note that constraint (10h) is equivalent to the following set of linear constraints

$$\sum_t y_{tmn} \leq M_1 \chi_{mn}, \quad \forall m, \forall n, \quad (11a)$$

$$\sum_t y_{tmn} \geq (1 - M_2) \chi_{mn}, \quad \forall m, \forall n, \quad (11b)$$

$$\sum_m \chi_{mn} \leq 1, \quad \forall n, \quad (11c)$$

where  $\chi_{mn}$ ,  $M_1$  and  $M_2$  are auxiliary variables so  $\chi_{mn} \in [0, 1]^{M \times N}$ ,  $M_1 \gg 1$  and  $0 < M_2 < 1$ , with  $M_1, M_2 \in \mathbb{R}$ . This transformation, based on the Big-M method, allows us to reformulate the constraint (10h) into an equivalent linear form, rendering the problem tractable.

#### IV. RIS-AWARE NETWORK PLANNING

In the following, we leverage on the 3D Beam Broadening and Flattening method [59]. While this technique is formulated originally for continuous phase shifts, works as [60], [61] ensure its applicability to more practical, discrete devices. Although in those papers we can see the production of

precise beams employing a reduced number of discrete phases, doing fine changes in the phase of the beam, as required for the Beam Broadening and Flattening method, is also an accessible technique. While the phase of the elements can only receive coarse changes (the quantized phase steps), we can change the original, continuous phase by an arbitrary (non-quantized) amount before rounding for discretization. This has the same effect as changing the same amount the phases of the elements, except for the small discretization errors as shown in those works. We employ this Beam Broadening and Flattening technique to decouple the RISs configuration from the BSs beamformers and produce an approximate formulation of the aforementioned problem. As the resulting problem is still highly complex and  $\mathcal{NP}$ -Hard, we rely on BCA and devise RISA as an iterative algorithm with proved convergence guarantees.

#### A. 3D Beam Broadening and Flattening Approximation

Even disregarding the interference, Problem (1) is still highly complex due to its objective function in Eq. (10a) being the sum of non-convex elements, and the binary constraints in Eq. (10j) that make it combinatorial. Moreover, as already mentioned in Section III-B, the lack of knowledge about the instantaneous UEs CSIs in the target area during a realistic access procedure invalidates the option of jointly configuring the RISs and BSs beamformers per UE [62]. Therefore, we decouple the RISs and BSs beamforming configurations from the planning problem itself by configuring each RIS to provide coverage to one contiguous subarea and assuming that each BS radiates all its available power towards each of its associated RISs in a time-division fashion. In other words, we assume that the RISs have a single-beam radiation pattern and that they do not serve more than one subarea, thereby guaranteeing that all locations belonging to one subarea are served by a single BS through one single RIS. Given sufficient coverage in the area, multiple users in each subarea can be separated by conventional OFDMA. This, together with the narrow-band of existing RISs devices [63], imposes the main limitation of the deployment we describe: the uplink and downlink connections will be limited by those the BS associated with the RIS is able to maintain within the RIS bandwidth and the employed multiple access method.

It can be easily observed from Eq. (9) that the SNR at UE  $\mathbf{u}_t$  provided by BS  $m$  through RIS  $n$  can be equivalently written as  $\text{SNR}(\Phi_n, \mathbf{w}_m, \mathbf{u}_t) = \frac{g_1(\Phi_n, \mathbf{w}_m, \mathbf{u}_t)}{g_2(\mathbf{u}_t)}$ , where  $g_1(\Phi_n, \mathbf{w}_m, \mathbf{u}_t)$  provides the overall array gain due to the cascaded active and passive beamformings, while  $g_2(\mathbf{u}_t)$  accounts for the concatenated BS-RIS-UE pathloss. Following [59], the RIS configuration can be obtained by means of 3D beam broadening and flattening, namely by partitioning the RIS into multiple sub-arrays of smaller size and optimizing their phase shifts to shape one single flattened beam whose beamwidth can be properly tuned to match the size of the target subarea. In particular, by denoting the subarea covered by RIS  $n$  by  $\mathcal{A}_n$  and assuming  $\mathbf{u}_t \in \mathcal{A}_n$ , the resulting BS-RIS gain can be written as

$$g_1(\Phi_n, \bar{\mathbf{w}}_m, \mathbf{u}_t) \approx \frac{N_h^2}{\Delta_{n,x'} N_h \delta} \frac{N_v^2}{\Delta_{n,y'} N_v \delta}, \quad \forall \mathbf{u}_t \in \mathcal{A}_n, \quad (12)$$



where  $\bar{\Phi}_n$  is derived by means of beam broadening and flattening, and  $\mathbf{w}_m$  is the maximum ratio transmission precoder, which depends only on  $\mathbf{G}_{mn}$ . Besides,  $\Delta_{n,x'}$  and  $\Delta_{n,y'}$  respectively denote the desired spans of the spatial frequency deviations along the horizontal  $x'_n$  and vertical  $y'_n$ -axis of RIS  $n$  to cover its subarea and are defined as

$$\Delta_{n,x'} \triangleq \max_{\mathbf{u}_t \in \mathcal{A}_n} \Omega_{T,n}(\mathbf{u}_t) - \min_{\mathbf{u}_t \in \mathcal{A}_n} \Omega_{T,n}(\mathbf{u}_t), \quad (13)$$

$$\Delta_{n,y'} \triangleq \max_{\mathbf{u}_t \in \mathcal{A}_n} \Psi_{T,n}(\mathbf{u}_t) - \min_{\mathbf{u}_t \in \mathcal{A}_n} \Psi_{T,n}(\mathbf{u}_t). \quad (14)$$

The overall pathloss experienced by the UE at coordinates  $\mathbf{u}_t$  is given by

$$g_2(\mathbf{u}_t) = d_{mn}^\beta d_n^\beta(\mathbf{u}_t). \quad (15)$$

Therefore, we can state the following equivalent formulation for Problem (1), i.e.

*Problem 2 (Multi-RIS coverage enhancement - equivalent):*

$$\max_{\mathbf{x}, \mathbf{y}, \Delta_{x'}, \Delta_{y'}} \min_{\mathbf{u}_t \in \mathcal{A}} \sum_{m,n} y_{tmn} \frac{1}{\Delta_{n,x'} \Delta_{n,y'}} \frac{1}{d_{mn}^\beta d_n^\beta(\mathbf{u}_t)} \quad (16a)$$

$$\text{s.t.} \quad \sum_m y_{tmn} |\Omega_{T,n}(\mathbf{u}_t) - \Omega_{T,n}(\mathbf{u}_k)| \leq \Delta_{n,x'}, \quad \forall n, \forall \mathbf{u}_t, \mathbf{u}_k \in \mathcal{A}, \quad (16b)$$

$$\sum_m y_{tmn} |\Psi_{T,n}(\mathbf{u}_t) - \Psi_{T,n}(\mathbf{u}_k)| \leq \Delta_{n,y'}, \quad \forall n, \forall \mathbf{u}_t, \mathbf{u}_k \in \mathcal{A}, \quad (16c)$$

$$\Delta_{n,x'} \geq \frac{1}{N_h \delta}, \quad \Delta_{n,y'} \geq \frac{1}{N_v \delta}, \quad \forall n, \quad (16d)$$

$$(10d), (10e), (10f), (10g), (10h), (10i), (10j),$$

in which we define  $\Delta_{x'} \triangleq [\Delta_{1,x'}, \dots, \Delta_{N,x'}]$ ,  $\Delta_{y'} \triangleq [\Delta_{1,y'}, \dots, \Delta_{N,y'}]$  while we omit the constant terms. In this equivalent formulation, we introduce the constraints in Eqs. (16b) and (16c) in order to guarantee that each TP served by RIS  $n$  lies within the coverage determined by its spatial frequency span. In Eq. (16d), we enforce that the spatial frequency spans  $\Delta_{x'}$  and  $\Delta_{y'}$  are at least as wide as the minimum beamwidth obtained by considering only a single sub-array while performing the RISs configuration via beam broadening and flattening, as by [59]. Furthermore, by inspecting the above formulations for  $g_1(\bar{\Phi}_n, \bar{\mathbf{w}}_m, \mathbf{u}_t)$  and  $g_2(\mathbf{u}_t)$ , respectively in Eqs. (12) and (15), we ascertain that the BS-RIS associations are now dependent only on the BS-RIS distances. This is consistent with the operational constraints of most RISs technologies, which operate as narrow-band devices, despite B5G networks being wide-band. Nonetheless, constraint (10e) guarantees that each RIS should be assigned to a BS only if in front of each other, which averts the straightforward distance-based BS-RIS association policy.

*Theorem 1:* Problem 2 is  $\mathcal{NP}$ -Hard.

*Sketch of Proof:* Even the continuous relaxation of Problem 2 is  $\mathcal{NP}$ -Hard, being a multiple-ratio Fractional Programming problem [64]. Therefore, Problem 2 is  $\mathcal{NP}$ -Hard.

### B. RIS-Aware planning algorithm

Hereafter, we design our multi-RIS planning algorithm, i.e., RISA. Let us first consider a continuous relaxation of

#### Algorithm 1: RIS-Aware network planning (RISA)

```

Initialize  $\Delta_{n,x'} = \Delta_{n,y'} = 2$ ,  $n = 1, \dots, N$ 
repeat                                     Outer BCA loop
    Solve the continuous relaxation of Problem 2
    jointly for  $\mathbf{x}$  and  $\mathbf{y}$ 
    repeat                                 First inner BCA loop
        Solve the transformed problem in  $\Delta_{x'}$  for  $\mathbf{z}_{x'}$ 
        Solve the transformed problem in  $\Delta_{x'}$  for  $\Delta_{x'}$ 
    until convergence of objective function in Eq. (17)
    repeat                                 Second inner BCA loop
        Solve the transformed problem in  $\Delta_{y'}$  for  $\mathbf{z}_{y'}$ 
        Solve the transformed problem in  $\Delta_{y'}$  for  $\Delta_{y'}$ 
    until convergence of objective function in Eq. (17)
    for  $\Delta_{y'}$ 
until convergence of objective function Eq. (16a) in
    Problem 2
Round  $\mathbf{x}$  and  $\mathbf{y}$  to derive binary  $\mathbf{x}^*$  and  $\mathbf{y}^*$  as by
Section IV-B

```

Problem (2) by letting  $\mathbf{x} \in [0, 1]^N$  and  $\mathbf{y} \in [0, 1]^{T \times M \times N}$  in constraint (10j). We can tackle such problem by means of BCA, namely by iteratively solving the problem for one block of optimization variables while keeping all the others fixed. Notably, although non-convex in general, the continuous relaxation of the problem is jointly convex in the block of variables  $\mathbf{x}, \mathbf{y}$  while it is still non-convex neither in  $\Delta_{x'}$ , nor in  $\Delta_{y'}$ , as the respective objective functions are convex and their maximization leads to a non-convex problem *per se*. In order to solve the problem for  $\Delta_{x'}$  (or, similarly, for  $\Delta_{y'}$ ), we can rearrange Eq. (16a) as

$$\max_{\Delta_{x'}} \min_{\mathbf{u}_t} \sum_{m,n} \frac{y_{tmn}}{d_{mn}^2 d_n^2(\mathbf{u}_t) \Delta_{n,y'}} \frac{1}{\Delta_{n,x'}}, \quad (17)$$

and observe that the resulting subproblem belongs to the Fractional Programming umbrella, being Eq. (17) a *sum of functions of ratios*. Therefore, we can leverage on the Quadratic Transform [65] and write it equivalently as

$$\max_{\mathbf{z}_{x'}, \Delta_{x'}} \min_{\mathbf{u}_t} \sum_{m,n} \frac{y_{tmn}}{d_{mn}^2 d_n^2(\mathbf{u}_t) \Delta_{n,y'}} (2z_{n,x'} - z_{n,x'}^2 \Delta_{n,x'}), \quad (18)$$

where  $\mathbf{z}_{x'} \in \mathbb{R}^N$  is an auxiliary optimization variable. The resulting subproblem is now convex in  $\mathbf{z}_{x'}$  and in  $\Delta_{x'}$  separately, thus likewise solvable by means of a nested BCA.

Therefore, the solution of the continuous relaxation of Problem (2) consists of a double-nested BCA whose outer loop iteratively considers the three blocks of variables  $\mathbf{x}$  and  $\mathbf{y}$ ,  $\Delta_{x'}$ ,  $\Delta_{y'}$ , while its inner loops solve the subproblems in  $\Delta_{x'}$  and  $\Delta_{y'}$  by introducing auxiliary variables  $\mathbf{z}_{x'} \in \mathbb{R}^N$  and  $\mathbf{z}_{y'} \in \mathbb{R}^N$ , respectively. We would like to highlight that, by dealing with a convex problem at each stage, the double-nested BCA is guaranteed to converge to a stationary point [11].

**Binary solution and complexity analysis.** The binary deployment and association variables  $\mathbf{x}^*$  and  $\mathbf{y}^*$  are recovered from the relaxed solution by means of a heuristic approach. Let us define the weight  $w_n$  of each CS in the final solution as  $x_n \sum_{t,m} y_{tmn}$ , namely by considering the combined effect of deploying a RIS at such CS with its associated TPs. Hence,

we round the  $L$  elements of  $\mathbf{x}$  with the highest weights to 1 while setting the other  $N-L$  to 0. We now establish the binary associations  $\mathbf{y}^*$  by considering only activated CSs  $\mathbf{r}_n$  such that  $x_n^* = 1$ . In particular, we iteratively associate each TP  $\mathbf{u}_t$  to a deployed RIS by setting to 1 the highest element of  $\mathbf{y}$  among the ones satisfying constraints (10d), (10e), i.e. feasible when considering the BS and RIS orientations. Concurrently, we update the values of  $\Delta_{n,x'}$  and  $\Delta_{n,y'}$  to the minimum spatial frequency spans satisfying the constraints in Eqs. (16b), (16c). We further improve the rounded solution via local search: by tweaking a single element of  $x^*$  or  $y^*$  at a time, we generate new rounded solutions and assess their objective function values at little additional computational cost. Whenever a new solution exceeds the objective function value of the current best solution, it is selected as the new final rounded solution. Please note that each stage of RISA can be solved efficiently by means of the interior method with complexity  $O(v^{3.5} \log(1/\epsilon))$ , where  $v$  is the dimension of the current optimization variables space and  $\epsilon$  is the desired solution accuracy [66]. Besides, the binary rounding algorithm has a worst-case complexity of  $O(NT \log(T))$ , which is typically negligible compared to the complexity of a single stage of the BCA loops. We depict the overall high-level algorithm in Algorithm 1.

## V. MODEL-FREE RIS PLANNING

As described above, RISA builds upon the assumption of LoS channels, which facilitates the formulation of the RISs planning as an optimization problem (c.f. Problems 1 and 2). In this section, we introduce an alternative approach, dubbed as AI-RISA, which leverages on the 3D model of the deployment area to derive an alternative RL-based solution capable of tailoring the RISs planning to the actual propagation properties of the scenario. Such approach relies on samples of the environment obtained via ad-hoc RT simulations, thereby removing the assumption of free-space propagation and gaining generality by taking into account the details of the surroundings in which the network devices interact.

### A. Q-learning preliminaries

Let us commence with a brief overview of Q-learning as the underlying RL technique upon which we build the proposed AI-RISA solution. Given a set of states  $\mathcal{S}$  and a set of actions  $\mathcal{P}$ , Q-learning defines an agent that may pick and perform any of the available actions  $a \in \mathcal{P}$  on the environment while the latter reacts by transitioning from the current state  $\varsigma \in \mathcal{S}$  to the next state  $\varsigma' \in \mathcal{S}$ . A reward is associated to the result of executing any specific action in each state, and the Q-learning agent identifies the optimal action-selection policy by aiming to maximize its total collected reward during the training phase. In other words, the agent explores the environment until it learns which action to make under different circumstances, i.e. at different environment states. It is worth highlighting that Q-learning is a model-free RL technique, namely it does not need a model for the environment but solely leverages on a reward function to evaluate the agent actions. As a central reason to pick this RL method, Q-learning is guaranteed to

converge to the optimal policy whenever the environment is a finite Markov Decision Process, i.e. with finite sets  $\mathcal{S}$  and  $\mathcal{P}$ , and satisfies the Markov property under which the environment state is a sufficient statistic of the future by capturing all relevant information from the history.

**Training process.** The Q-learning technique revolves around a Q-table consisting of one row per state and one column per action, which is trained over various episodes obtained by randomly selecting an initial environment state. The overall Q-learning training process requires several training epochs, each including a collection of episodes. In particular, in each epoch, a fixed known number of episodes are carried out while the solution is refined on a per-epoch basis until convergence.

**Action selection.** The agent policy develops throughout each epoch. Specifically, the actions are fully randomized at the epochs beginning while becoming increasingly based on the current agent knowledge as training advances. Being the total duration of a given epoch  $T_E$ , an action taken at time  $t$  is exploratory, i.e. random and not based on the current agent knowledge, with probability  $P_{\text{explore}} = 1 - \left(\frac{t}{T_E}\right)^\tau$ . Conversely, it is exploitative, namely the agent selects the best known action for the current state, with probability  $P_{\text{exploit}} = \left(\frac{t}{T_E}\right)^\tau$ , where  $\tau \in \mathbb{R}^+$  determines how long the exploration remains dominant over the exploitation.

**Rewards and Q-table update.** The Q-table is typically initialized to random values, which are updated during training. As previously mentioned, a reward is assigned to performing an action on the environment in its current state, aiming at penalizing infeasible actions and evaluating transitions among states. Let us assume that the agent executes action  $a \in \mathcal{P}$  on the environment in state  $\varsigma \in \mathcal{S}$ , producing a transition to state  $\varsigma' \in \mathcal{S}$  with associated reward  $r(\varsigma, \varsigma') \in \mathbb{R}$ . Hence, the new Q-table entry  $Q'(\varsigma, a)$  for the state-action tuple  $\{\varsigma, a\}$  is updated as

$$Q'(\varsigma, a) = (1 - \alpha_q) Q(\varsigma, a) + \alpha_q \left[ r(\varsigma, \varsigma') + \gamma_q \max_{a \in \mathcal{P}} Q(\varsigma', a) \right], \quad (19)$$

where the learning rate  $\alpha_q$  controls how much newly obtained rewards affect the Q-table values,  $Q(\varsigma, a)$  indicates the previous Q-table value for the tuple  $\{\varsigma, a\}$ , and  $\gamma_q$  is the discount factor capturing the importance of future rewards on the new Q-table value (through the maximum Q-table value obtainable at state  $\varsigma'$ ). Infeasible actions can receive a negative reward (e.g., equal to  $-1$ ), thus discouraging the Q-learning algorithm from further considering them as candidate actions in the corresponding environment states.

### B. AI-RISA

In the following, we delve into the details of the proposed AI-RISA solution. By leveraging on Q-learning, AI-RISA allows directly tackling the RISs planning using as directive information only the metric by which we evaluate the candidate solutions. Thus, when solving the deployment in scenarios without LoS assumption, the approach will make use



**Algorithm 2: AI RIS-Aware network planning (AI-RISA)**

```

Cluster TPs in  $N_C$  clusters
Initialize deployment Q-table  $Q_D$ 
repeat
  for deployment epoch = 0,1,2... do
    Pick a random deployment state  $\varsigma_D$ 
    repeat
      Pick a deployment action  $a_D$ 
      Initialize association Q-table  $Q_A$ 
      for association epoch = 0,1,2... do
        Pick a random association state  $\varsigma_A$ 
        repeat
          Pick an association action  $a_A$ 
          Compute  $v(\varsigma_A, \varsigma_D)$  using RT
          Compute  $r(\varsigma_A, \varsigma'_A)$ 
           $Q'_A(\varsigma_A, a_A) \leftarrow f(Q_A(\varsigma_A, a_A), r(\varsigma_A, \varsigma'_A))$ 
        until episode end
      end
       $v(\varsigma_D) \leftarrow \max_{\varsigma_A} v(\varsigma_A, \varsigma_D)$ 
      Compute  $r(\varsigma_D, \varsigma'_D)$ 
       $Q'_D(\varsigma_D, a_D) \leftarrow f(Q_D(\varsigma_D, a_D), r(\varsigma_D, \varsigma'_D))$ 
    until episode end
  end
until convergence of  $\max_{\varsigma_D} (v(\varsigma_D))$ 

```

of the propagation information with minimal assumptions, i.e. by replacing the free-space pathloss  $d_{mn}^{-\beta} d_n^{-\beta}(\mathbf{u}_t)$  in Eq. (16a) with the attenuation value obtained via ad-hoc simulations. To this aim, we develop an ad-hoc RT simulator that takes as input the 3D model of the target area, and for each candidate network topology derives the received power at any given point. We will describe in detail the RT later in Section VI.

**Framework overview.** As depicted in Fig. 3, our proposed RL-based architecture is divided into a pre-processing stage of the TPs and two nested layers of Q-learning solvers. In the pre-processing, we cluster the TPs based on their spatial location. Then, considering only complete clusters of TPs we search for the best deployment using the nested agents. With the agent in the outer layer, we scan possible deployments, i.e. which  $L$  candidate sites will be equipped with a RIS out of the total number of  $N$ , and for each deployment, we use the agent in the inner layer to search for the best association, i.e. which RIS will cover each TPs cluster. On each layer of Q-learning solving we employ a separate algorithm with independent training processes and Q-tables.

For each solution probed in the outer layer (candidate deployments), we perform a complete run of the inner agent training to find the best association for that deployment. The association agent calls a simulation routine for each probed association, which evaluates the complete scenario using the parameters of both sides of the candidate solution (deployment and associations) and RT data. We feed the obtained metric back to the inner layer agent to obtain the best association and use the metric of the best association found as feedback to the outer solver, so we can derive the best deployment. We

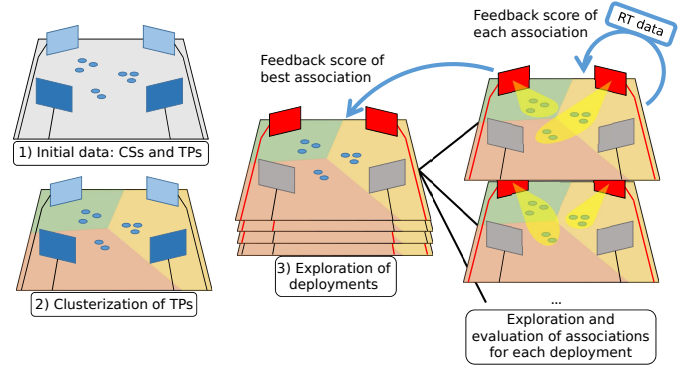


Fig. 3: Overview of AI-RISA process blocks

set said evaluation metric as the minimum SNR of any given TP to obtain results comparable with those obtained from RISA, though this might be altered to improve the solution with negligible computational cost, e.g., by evaluating the average SNR improvements when the agent cannot improve the minimum SNR. Note that we take as the solution the states found during the training stages with the best values for our metric, disregarding the characteristics or behaviour finally gained by the agent after the training.

**TP clusterization.** In this step we use the BIRCH algorithm [67] to group the given TPs in  $N_C$  spatially defined clusters, with  $N_C \geq N$ , such that there is at least one cluster per deployed RIS. This allows us to solve scenarios handling large amounts of TPs without the size of the solution space growing out of tractability. By performing such preprocessing, we open the possibility of designating many TPs, ensuring the solver performs a thorough evaluation of the solutions while keeping the problem workable. Setting a low number of clusters can nevertheless limit the ability of the agent to find an optimal solution as all points in a cluster have to be assigned to the same RIS. The BIRCH algorithm is capable of producing workable clusters even with homogeneously distributed or tightly grouped TPs. Since we use it to produce a fixed amount  $N_C$  of sets, it always keeps the data tractable during the exploration stages of the solution.

**Outer layer.** In our model, the states on the outer layer correspond to all possible combinations of  $L$  or less RISs deployed with a total number of  $\sum_{i=0}^L C(N, i) = \sum_{i=0}^L \frac{N!}{i!(N-i)!}$ , where  $C(n, k)$  denotes the number of  $k$ -combinations from a given set of  $n$  elements. Since any evolution of complete states (i.e., states where there are  $L$  RISs deployed) will forcefully withdraw the deployment to an incomplete state first, in this layer we favour incomplete states (where the number of deployed RISs is still below the limit  $L$ ) as the initial state of each training episode by setting the probability of starting an episode from an incomplete state above the probability of starting from a complete state:  $P_{incomplete} > P_{complete}$ .

The set of actions we define for this agent comprises: *i*) deploying a RIS at a given CS, which we consider an invalid action if there are  $L$  RISs already deployed or if the CS picked is already in use; *ii*) withdrawing a deployed RIS from a given CS, which we consider an invalid action if there is no RIS deployed in that CS or if the limit of  $L$  RISs was not already reached; *iii*) concluding the evolution of the state, offering

TABLE I: Simulation and Q-learning parameters.

Parameter	Value	Parameter	Value	Parameter	Value
$P$	28 dBm	$f$	26 GHz	$\sigma^2$	-80 dBm
$\beta$	2	$\mu$	0.5	$A$	100 m $\times$ 100 m
BSs ( $M$ )	2	CSs ( $N$ )	{10,20,30}	$T$	16
$N_b$	2	$N_r$	350 $\times$ 175	$N_{ref}$	2
$\tau$	1	$\alpha_q$	0.5	$\gamma_q$	0.99
SNR <sub>max</sub>	10 dB	$P_{complete}$	0.2	$P_{incomplete}$	0.8

the current state as a candidate solution. Invalid actions do not trigger any state evolution.

**Inner layer.** Following the same framework, we list the states on the inner layer as all possible associations of the RISs to TPs, which gives us a total of  $L^{N_C}$  possible states. The set of actions we define for this agent comprises: *i*) associating the cluster  $n_C$  to the next entry in the deployed RIS list; *ii*) associating the cluster  $n_C$  to the previous entry in the deployed RIS list; *iii*) concluding the evolution of the state, considering the present state as a candidate solution. As all actions in this list will be feasible for any given deployment and association, we do not consider any action invalid for the association agent.

**Rewards.** Defining the reward for each action considered invalid in the outer layer we further discourage the agent from choosing those (as they provide no evolution for the state). For all other actions, considered valid, we run the association solver and use the metric of the best solution found. We then reward the outer layer agent by taking the difference in the evaluation metric between the prospective state and the current state. As for the inner layer, since there is no invalid action in the agent space, the reward always comes from computing the difference in the evaluation of the prospective state and the current.

## VI. PERFORMANCE EVALUATION

We first evaluate RISA and AI-RISA via Monte Carlo simulations considering synthetic network topologies and benchmark them against the SOA solution in [10] and two ES approaches. Subsequently, we test RISA, AI-RISA and the same ES techniques on the real network topology installed in the *Rennes railway station*, France, provided by the European network operator *Orange*, wherein RISs CSs are properly placed on the station floor plan, as described in Section III-B, and realistic SNR values are obtained via ray tracing.

Simulation parameters based on realistic values are listed in Table I, unless otherwise stated.

**RIS-aware RT simulator.** Hereafter we outline the features of our RT simulator, which is a key component of the reward function in AI-RISA and is fundamental to assess the network performance in the Rennes railway station scenario. We employ the well-known shooting and bouncing ray (SBR) method, which *i*) emits rays from each transmitter in a dense grid, covering the surrounding sphere, *ii*) propagates the rays through the geometric environment according to Snell's law and adjusts their electromagnetic field in light of Fresnel's coefficients, *iii*) evaluates the received power at any given point by summing up the power of the electromagnetic fields of each ray reaching such point or its vicinity [68]. As SBR suffers from high uncertainty on ray paths, which translates on non-negligible phase errors especially at mm-Wave frequencies, we consider each ray to have a random phase uniformly drawn from the interval  $[0, 2\pi)$  [69].

We would like to underline that RISs are novel network devices, thereby not yet widely implemented in conventional RT. Therefore, we devise a new lightweight technique to compute the contribution of these devices to the transmission by considering the impinging power on the RIS surface, the RIS power reflection, and the RIS beampattern. To estimate the impinging power on the RIS surface, we assess the power received at the RIS center by one of its elements modeled as a cosine antenna (with exponent parameter  $\mu = 0.5$ ) and multiply this value by the number of RIS elements  $N_r$ . Hence, we simulate the RIS controlled reflections by considering outgoing rays originated on the RIS surface with power equal to the RIS impinging power. As for the RIS emissive beampattern, we can consider a plethora of different approaches, e.g. *i*) the RIS is focused on a set of points and modeled as a uniform rectangular array of  $N_r$  cosine antenna whose static configuration is obtained by narrow-band phase-shift beamforming, *ii*) the RIS is dynamically configured to focus on each individual point in the service area and its beampattern is derived by combining the highest achievable gain in each reflection direction, *iii*) the RIS is statically configured to cover the service area by means of beam broadening and flattening while its beampattern is a step function discriminating if a direction  $\mathbf{u}_t$  belongs to a given subarea  $\mathcal{A}_n$ . In our scenario, the model in *i*) requires solving a complex optimization problem to derive the optimal RIS configuration that simultaneously serves multiple UEs in the area, while the approach in *ii*) implies perfect instantaneous RIS reconfiguration capabilities, which is difficult to achieve in realistic conditions. Therefore, we adopt the model in *iii*) to numerically evaluate all solutions in a practical manner, namely we define the RIS beampattern  $g(\mathbf{u})$  as

$$g(\mathbf{u}) = \begin{cases} g_1 & \text{if } \mathbf{u}_t \in \mathcal{A}_n \quad (\text{cf. Eq. (12)}), \\ 0 & \text{if } \mathbf{u}_t \notin \mathcal{A}_n. \end{cases} \quad (20)$$

Lastly, we compute the received power at each TP by adding up the power from each source of any incident ray as received by an isotropic antenna placed at the TP coordinates. Note that we assume a power-based association policy, namely we consider each TP to be associated to the BS providing the highest power, combining the direct link and the reflections through the deployed RISs.

**Comparison benchmarks.** In the following, we describe the design choices while implementing the performance benchmarks. The solution proposed in [10] provides a Mixed Integer Linear Programming (MILP) formulation of the RIS-aided coverage planning problem solely leveraging on geometrical considerations and the availability and quality of the links attainable between CSs and TPs. For a homogeneous comparison we adapt this solution to match the operating conditions of RISA and AI-RISA: we fix the orientation of the CSs, and the number and position of the BSs, while the original method counts those among the variables to be optimized. After obtaining a solution for the deployment and association subproblems, we compute the gain that the RISs would exhibit in those conditions according to Eq. (12), and evaluate the solution with the same reward function used for

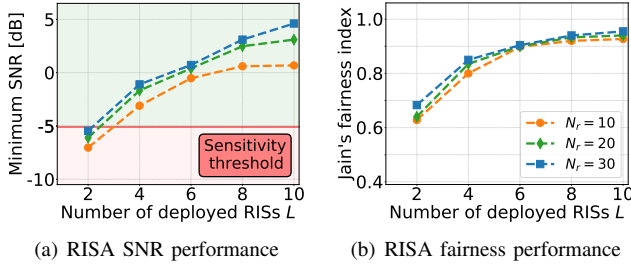


Fig. 4: RISA performance with different numbers of deployed RISs and available Candidate Sites (CSs) via Monte Carlo simulations considering synthetic topologies.

all the solutions under scrutiny. Note that the difference in performance between the method we propose and the SOA we are comparing with should be in part attributed to the latter being a generalist deployment method, while the former targets the specific conditions of the scenario here evaluated (e.g. the RISs covering all their linked TPs at the same time). When performing ES, the total space of possible solutions grows out of tractability at very small numbers as the total number of solutions is  $\frac{N!}{L!(N-L)!}L^T$ , where  $N$  is the number of candidate sites,  $L$  is the number of deployed RISs and  $T$  is the number of TPs. Therefore, we present the ES solution together with a *clustered exhaustive search*: in this method, we first cluster the points using the BIRCH algorithm [67] as described in the first step of AI-RISA, and then apply an ES algorithm over the space of solutions that associates complete clusters of TPs to the RISs. This method represents a high-cost solution but also reveals the least upper bound for the scores attainable by AI-RISA and helps to judge the impact of the loss of generality incurred by the clustering step.

**Synthetic topologies.** We consider the target area to be a square surface with area  $A = 100\text{m} \times 100\text{m}$ . Besides, we assume that  $M = 2$  BSs are placed at the bottom-left and upper-right corners of the area, namely  $\mathbf{b}_1 = [0, 0, 5.5]^T$ ,  $\mathbf{b}_2 = [100, 100, 5.5]^T$ , while we evaluate the SNR performance at  $T = 16$  TPs uniformly distributed in the target area on the plane  $z = 1.5$ . We average the results over  $10^3$  Monte Carlo executions. In Fig. 4(a), we show the RISA performance in terms of minimum SNR experienced in the target area with respect to the number of deployed RISs  $L$  for different numbers of available CSs  $N = \{10, 20, 30\}$  on the plane  $z = 5.5$ . Comparison against AI-RISA is not included, as the execution time for the training stage grows out of feasibility for this experiment. The horizontal line indicates the minimum SNR threshold to meet the receiver sensitivity. As expected, the minimum SNR shows a positive monotonic behavior with decreasing relative increments, thus suggesting the existence of an optimal value for  $L$ . Besides, increasing the number of CSs does not significantly benefit the overall performance, provided that the number of CSs is big enough to obtain a good sampling of the target area (on average). We employ the Jain's fairness index (JFI) to evaluate the SNR fairness among TPs [70]. However, we modify its formulation by introducing

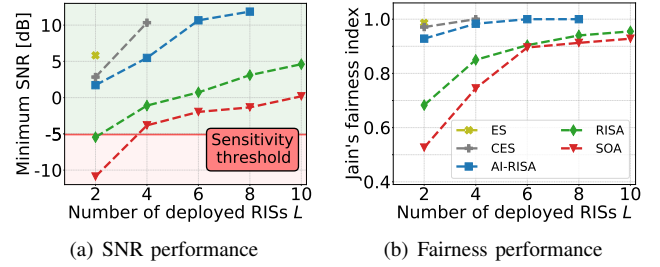


Fig. 5: RISA and AI-RISA performance against SOA [10] (adapted to our scenario), ES and clustered exhaustive search (CES) with different numbers of deployed RISs via Monte Carlo simulations considering synthetic topologies.

a saturation value of  $\text{SNR}_{\max} = 10\text{dB}$ , namely

$$\text{JFI}_{\text{saturated}}(\text{SNR}_1, \text{SNR}_2, \dots, \text{SNR}_T) = \frac{(\sum_{t=1}^T \min(\text{SNR}_t, \text{SNR}_{\max}))^2}{T \cdot \sum_{t=1}^T (\min(\text{SNR}_t, \text{SNR}_{\max}))^2}, \quad (21)$$

where  $\text{SNR}_t$  indicates the SNR experienced at TP  $\mathbf{u}_t$ . This way, we are able to capture the fairness in the access to a sufficient SNR level preventing higher SNR values (e.g., for TPs in the immediate vicinity of a RIS) from artificially decreasing the fairness value. In this regard, Fig. 4(b) outlines a positive monotonic trend, validating our *max-min* objective function design choice to enhance coverage in the whole area.

**RISA and AI-RISA evaluation with synthetic traces.** Fig. 5 depicts the RISA and AI-RISA performance against the SOA solution from [10] against the number of deployed RISs. The proposed AI-RISA, based on Q-learning, is feasible with reasonable hardware resources up to  $L = 8$ , while RISA is able to surpass this limitation. As an additional comparison term, we include the ES solution, which is computationally feasible only up to  $L = 2$  deployed RISs, and the CES solution, feasible up to  $L = 4$ . In order to perform a sound comparison, we reward the AI-RISA agent with the same objective function as RISA in Eq. (16a), thus tackling Problem 2 without further approximations or simplifications. As shown in the figure, all solution trends in terms of SNR and JFI match significantly with the increase of the number of deployed RISs. We would like also to stress that the nature of the underlying Q-learning technique guarantees convergence for AI-RISA to the same results as the (clustered) ES given sufficient time [71]. Such convergence depends in practice on the available training time and the convergence criteria. Furthermore, it is worth mentioning that the CES finds comparable solutions to those of the ES, hence supporting the idea that the loss of generality due to the clusterization step impacts the quality of the solutions to a limited extent. While a strict complexity analysis is not feasible due to the usage of third party convex programming tools in our solutions, we can report the observed execution times until completion (for exhaustive searches) or until convergence (for RISA and AI-RISA). Our test platform is a server equipped with 2x Intel® Xeon® Processor E5-2650 v4 and 160GB of DDR4 memory. RISA and AI-RISA execution time [in hours] in the described circumstances grows approximately as  $\tau L$ , with  $\tau \approx 0.8\text{h}$ . The

ES and CES execution time grows with  $L!$ , going from 2h for  $L = 2$  to around 30h for  $L = 4$ , and becoming impractical beyond that point.

**Rennes station.** We execute the RT simulation in MATLAB R2021b using a simplified 3D model of the main floor of the Rennes railway station in France. The scenario follows the most prominent obstacles and elements filling the volume object of study. Our initial reproductions of the interior of the station, based primarily on the architectural plans, attempted to produce an architecturally faithful model. Nevertheless, the results obtained when processing those through ray tracing failed in the most important metric: accurately predicting the propagation conditions observed through measurements in the actual environment of the station. The main source of disagreement was that the reflections in the ceiling, crowded with small curved surfaces, were not well represented in a polygon-based model. We tested several options, mostly trying to accurately represent the absorption properties of the materials present in the ceiling. The higher the absorption properties assigned to the many structural, functional, and decorative beams, as well as tubing and other elements in the ceiling, the more accurately our simulations resembled the observed propagation conditions in the station. As we obtained the best reproduction of the propagation conditions observed in the station (i.e., the areas of coverage problems) by making them perfect absorbers, we opted for the -mathematically equivalent- omission of the ceiling in the model, negating any reflection on it back to the environment. The resulting model has 579 triangles, 1582 edges and 1053 vertexes and is depicted in Fig. 1. The use of this detailed model makes the evaluations of the solutions aware of the presence of scatterers and allows us to take into consideration the signal fading. We simulate the BSs with  $N_b = 2$  and transmit power  $P = 28$  dBm at  $f = 26$  GHz, as in the real network deployment by *Orange*. Besides, we implement the SBR method in order to derive the possible paths to reach any given TP [72]. We linearly combine the power received at any TP from different paths assuming a (uniformly distributed) random phase for each individual path at the UE side, thereby accounting for random external factors (e.g., thermal expansion) that could alter the path lengths by a non-negligible fraction of a wavelength  $\lambda = 1/f$ , given the large ratio between the station distances and the wavelength [69]. The maximum number of reflections is set to  $N_{ref} = 2$  as higher-order reflections provide little contribution to the received power.

In Fig. 6, we show the RISA and AI-RISA performance for different numbers of deployed RISs among  $N = 20$  hand-picked CSs at a height of 5.5 m and meeting the architectural constraints of the station building and internal structures. Besides, we compare such results with a random deployment policy averaged over  $10^2$  instances, and the SOA, ES, and CES methods used in the synthetic scenarios. Clearly, RISA and AI-RISA outperform the random policy, the SOA, ES and CES methods in the maximized metric, i.e., minimum SNR in Fig. 6(a), and outperform the same solutions in almost all deployments regarding the JFI in Fig. 6(b). Note how, while the minimum SNR (i.e., our optimization objective) grows monotonically, this is not always the same for the JFI: several

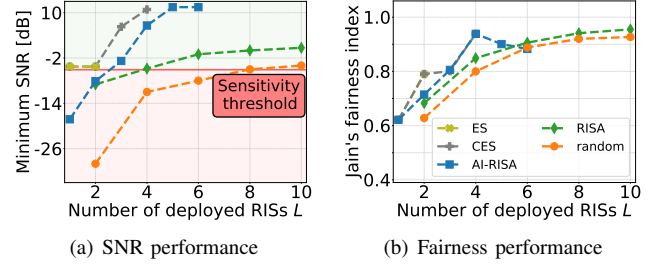


Fig. 6: RISA and AI-RISA performance obtained via RT simulations for different numbers of deployed RISs and available Candidate Sites (CSs) in a realistic environment (Rennes station), compared to CES, ES, and random solutions.

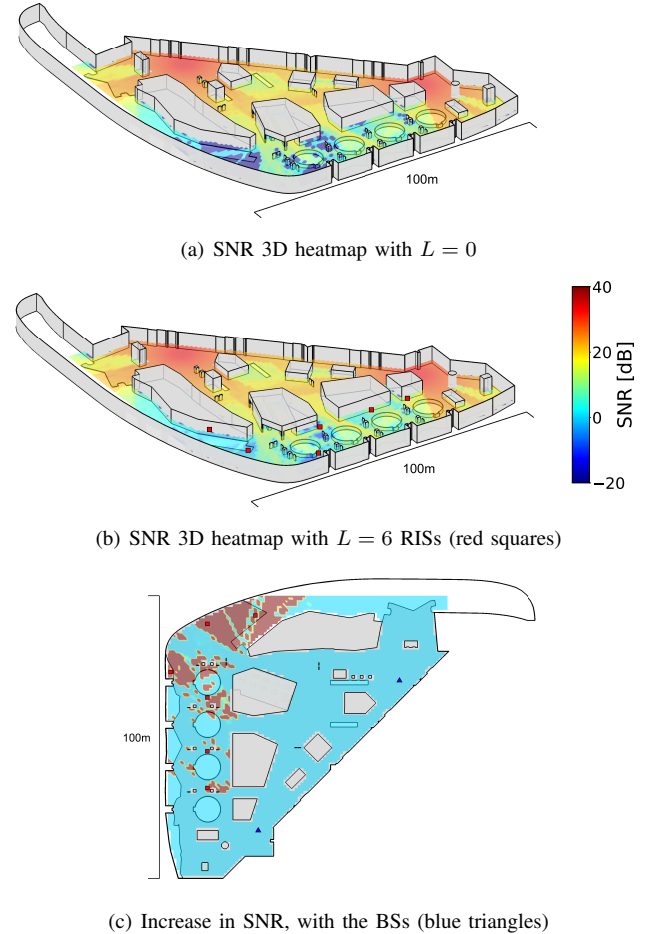


Fig. 7: SNR heatmap in the dead-zone (see Figure 1) of the Rennes station obtained via RT simulations.

scenarios (e.g. an increase in the worse covered points which is accompanied by an even higher increase of the better covered points, or an increase in the worst covered point that turns it into a high outlier) produce a decrease in the JFI as the one observed for  $L = \{5, 6\}$  in the AI-RISA series. The fairness is further confirmed in Fig. 7, wherein we compare the 3D heatmaps of the SNR for  $L = 6$  numbers of deployed RISs against the baseline with no RIS.



## VII. CONCLUSIONS

Reconfigurable intelligent surfaces introduce a novel challenge in traditional cellular networks planning. On the one hand, optimal RISs configurations should be computed given fixed BSs and RISs positions. On the other hand, the optimal RISs deployment depends on RISs configurations. To address this coupled problem and make the analysis tractable, in this paper we proposed two RIS-aware network planning solution: RISA, which builds on double-nested block coordinate ascent to iteratively tackle the above challenge, and AI-RISA, which uses several ML techniques and a RT simulator to find the optimal solution. RISA and AI-RISA are evaluated on synthetic generic indoor network deployments and in a real railway station (Rennes). Our results show that RISA and AI-RISA can *i*) achieve outstanding performance on top of the existing network infrastructure, *ii*) solve the dead-zone problem in highly-crowded environments and *iii*) improve the user fairness at very limited installation costs.

## VIII. ACKNOWLEDGEMENTS

This work was supported by EU H2020 RISE-6G (grant agreement 101017011) and EU H2020 METAWIRELESS (grant agreement 956256) projects. We thank Stéphane Ros, with Société nationale des chemins de fer français, 93210 Saint-Denis, France, for the assistance.

## REFERENCES

- [1] A. Albanese, G. Encinas Lago, V. Sciancalepore, X. Costa-Pérez, D.-T. Phan-Huy, and R. Stéphane, "RIS-Aware Indoor Network Planning: The Rennes Railway Station Case," in *IEEE ICC 2022 - IEEE International Conference on Communications*, 2022.
- [2] M. Di Renzo, A. Zappone, M. Debbah, M.-S. Alouini, C. Yuen, J. de Rosny, and S. Tretjakov, "Smart Radio Environments Empowered by Reconfigurable Intelligent Surfaces: How It Works, State of Research, and The Road Ahead," *IEEE Journal on Selected Areas in Communications*, vol. 38, no. 11, pp. 2450–2525, 2020.
- [3] M. Di Renzo, M. Debbah, D.-T. Phan-Huy, A. Zappone, M.-S. Alouini, C. Yuen, V. Sciancalepore, Alexandropoulos *et al.*, "Smart radio environments empowered by reconfigurable AI meta-surfaces: an idea whose time has come," *EURASIP Journal on Wireless Communications and Networking*, vol. 2019, no. 1, pp. 1–20, May 2019.
- [4] G. C. Trichopoulos, P. Theofanopoulos, B. Kashyap, A. Shekhawat, A. Modi, T. Osman, S. Kumar, A. Sengar, A. Chang, and A. Alkhateeb, "Design and Evaluation of Reconfigurable Intelligent Surfaces in Real-World Environment," *IEEE Open Journal of the Communications Society*, vol. 3, pp. 462–474, 2022.
- [5] A. Albanese, F. Devoti, V. Sciancalepore, M. Di Renzo, and X. Costa-Pérez, "MARISA: A Self-configuring Metasurfaces Absorption and Reflection Solution Towards 6G," in *IEEE INFOCOM 2022 - IEEE Conference on Computer Communications*, 2022.
- [6] F. Tariq, M. R. A. Khandaker, K.-K. Wong, M. A. Imran, M. Bennis, and M. Debbah, "A Speculative Study on 6G," *IEEE Wireless Communications*, vol. 27, no. 4, pp. 118–125, 2020.
- [7] A. Ptilakis, O. Tsilipakos, F. Liu, K. M. Kossifos, A. C. Tasolamprou, D.-H. Kwon, M. S. Mirmoosa, D. Manassis, N. V. Kantartzis, Liaskos *et al.*, "A Multi-Functional Reconfigurable Metasurface: Electromagnetic Design Accounting for Fabrication Aspects," *IEEE Transactions on Antennas and Propagation*, vol. 69, no. 3, pp. 1440–1454, 2021.
- [8] J. G. Andrews, F. Baccelli, and R. K. Ganti, "A Tractable Approach to Coverage and Rate in Cellular Networks," *IEEE Transactions on Communications*, vol. 59, no. 11, pp. 3122–3134, 2011.
- [9] A. Fascista, A. Coluccia, H. Wymeersch, and G. Seco-Granados, "Millimeter-Wave Downlink Positioning With a Single-Antenna Receiver," *IEEE Transactions on Wireless Communications*, vol. 18, no. 9, pp. 4479–4490, 2019.
- [10] E. Moro, I. Filippini, A. Capone, and D. De Donno, "Planning Mm-Wave Access Networks With Reconfigurable Intelligent Surfaces," in *2021 IEEE 32nd Annual International Symposium on Personal, Indoor and Mobile Radio Communications (PIMRC)*, 2021, pp. 1401–1407.
- [11] L. Grippo and M. Sciandrone, "On the Convergence of the Block Nonlinear Gauss-Seidel Method under Convex Constraints," *Operations Research Letters*, vol. 26, no. 3, p. 127–136, Apr. 2000.
- [12] S. Hurley, "Planning effective cellular mobile radio networks," *IEEE Transactions on Vehicular Technology*, vol. 51, no. 2, pp. 243–253, 2002.
- [13] L. Huang, Y. Zhou, X. Han, Y. Wang, M. Qian, and J. Shi, "Distributed coverage optimization for small cell clusters using game theory," in *2013 IEEE Wireless Communications and Networking Conference (WCNC)*, 2013, pp. 2289–2293.
- [14] G. Koutittas, A. Karousos, and L. Tassioulas, "Deployment Strategies and Energy Efficiency of Cellular Networks," *IEEE Transactions on Wireless Communications*, vol. 11, no. 7, pp. 2552–2563, 2012.
- [15] T. X. Brown, "Cellular performance bounds via shotgun cellular systems," *IEEE Journal on Selected Areas in Communications*, vol. 18, no. 11, pp. 2443–2455, 2000.
- [16] L. Chiaraviglio, G. Bianchi, N. Blefari-Melazzi, and M. Fiore, "Will the proliferation of 5G base stations increase the radio-frequency 'pollution'?" in *IEEE 91st Vehicular Technology Conference (VTC2020-Spring)*, 2020.
- [17] J. T. J. Penttinen, "5G Network Planning and Optimization," in *5G Explained: Security and Deployment of Advanced Mobile Communications*, 2019, pp. 255–269.
- [18] A. Albanese, V. Sciancalepore, A. Banchs, and X. Costa-Pérez, "LOKO: Localization-aware Roll-out Planning for Future Mobile Networks," *IEEE Transactions on Mobile Computing*, pp. 1–1, 2022.
- [19] L. Chiaraviglio, A. S. Cacciapuoti, G. D. Martino, M. Fiore, M. Montesano, D. Trucchi, and N. B. Melazzi, "Planning 5G Networks Under EMF Constraints: State of the Art and Vision," *IEEE Access*, vol. 6, pp. 51 021–51 037, 2018.
- [20] F. Devoti and I. Filippini, "Planning mm-Wave Access Networks Under Obstacle Blockages: A Reliability-Aware Approach," *IEEE/ACM Transactions on Networking*, vol. 28, no. 5, pp. 2203–2214, 2020.
- [21] I. Filippini, V. Sciancalepore, F. Devoti, and A. Capone, "Fast Cell Discovery in mm-Wave 5G Networks with Context Information," *IEEE Transactions on Mobile Computing*, vol. 17, no. 7, pp. 1538–1552, 2018.
- [22] A. L. Rezaabad, H. Beyranvand, J. A. Salehi, and M. Maier, "Ultra-Dense 5G Small Cell Deployment for Fiber and Wireless Backhaul-Aware Infrastructures," *IEEE Transactions on Vehicular Technology*, vol. 67, no. 12, pp. 12 231–12 243, 2018.
- [23] D. López-Pérez, M. Ding, H. Claussen, and A. H. Jafari, "Towards 1 Gbps/UE in Cellular Systems: Understanding Ultra-Dense Small Cell Deployments," *IEEE Communications Surveys and Tutorials*, vol. 17, no. 4, pp. 2078–2101, 2015.
- [24] H. Wang, X. Zhou, and M. C. Reed, "Coverage and Throughput Analysis with a Non-Uniform Small Cell Deployment," *IEEE Transactions on Wireless Communications*, vol. 13, no. 4, pp. 2047–2059, 2014.
- [25] A. Dong, X. Luo, and Q. Du, "A small cell deployment strategy towards amorphous coverage in the cellular network," in *2015 International Wireless Communications and Mobile Computing Conference (IWCMC)*, 2015, pp. 745–750.
- [26] J. Y. Han, O. Jo, and J. Kim, "Exploitation of Channel-Learning for Enhancing 5G Blind Beam Index Detection," *IEEE Transactions on Vehicular Technology*, vol. 71, no. 3, pp. 2925–2938, 2022.
- [27] G. H. Sim, S. Klos, A. Asadi, A. Klein, and M. Hollick, "An Online Context-Aware Machine Learning Algorithm for 5G mmWave Vehicular Communications," *IEEE/ACM Transactions on Networking*, vol. 26, no. 6, pp. 2487–2500, 2018.
- [28] M. Alrabeiah and A. Alkhateeb, "Deep Learning for mmWave Beam and Blockage Prediction Using Sub-6 GHz Channels," *IEEE Transactions on Communications*, vol. 68, no. 9, pp. 5504–5518, 2020.
- [29] C. Pan, H. Ren, K. Wang, J. F. Kolb, M. Elkhachan, M. Chen, M. Di Renzo, Y. Hao, J. Wang, A. L. Swindlehurst, X. You, and L. Hanzo, "Reconfigurable Intelligent Surfaces for 6G Systems: Principles, Applications, and Research Directions," *IEEE Communications Magazine*, vol. 59, no. 6, pp. 14–20, 2021.
- [30] H. Liu, J. Zhang, Q. Wu, H. Xiao, and B. Ai, "ADMM Based Channel Estimation for RISs Aided Millimeter Wave Communications," *IEEE Communications Letters*, vol. 25, no. 9, pp. 2894–2898, 2021.
- [31] R. Liang, J. Fan, and J. Yue, "A cascaded multi-IRSs beamforming scheme in mmWave communication systems," *IEEE Access*, vol. 9, pp. 99 193–99 200, 2021.

- [32] A. Albanese, V. Sciancalepore, and X. Costa-Perez, "SARDO: An Automated Search-and-Rescue Drone-based Solution for Victims Localization," *IEEE Transactions on Mobile Computing*, pp. 1–1, 2021.
- [33] M. Dunna, C. Zhang, D. Sievenpiper, and D. Bharadia, *ScatterMIMO: Enabling Virtual MIMO with Smart Surfaces*. Association for Computing Machinery, 2020.
- [34] L. Dai, B. Wang, M. Wang, X. Yang, J. Tan, S. Bi, S. Xu, F. Yang, Z. Chen, M. D. Renzo, C.-B. Chae, and L. Hanzo, "Reconfigurable Intelligent Surface-Based Wireless Communications: Antenna Design, Prototyping, and Experimental Results," *IEEE Access*, vol. 8, pp. 45 913–45 923, 2020.
- [35] J. Sung, J. Choi, and B. L. Evans, "Narrowband channel estimation for hybrid beamforming millimeter wave communication systems with one-bit quantization," in *2018 IEEE International Conference on Acoustics, Speech and Signal Processing (ICASSP)*. IEEE, 2018, pp. 3914–3918.
- [36] J. Tang, M. Cui, S. Xu, L. Dai, F. Yang, and M. Li, "Transmissive ris for b5g communications: Design, prototyping, and experimental demonstrations," *IEEE Transactions on Communications*, 2023.
- [37] C. Pan, H. Ren, K. Wang, W. Xu, M. Elkashlan, A. Nallanathan, and L. Hanzo, "Multicell mimo communications relying on intelligent reflecting surfaces," *IEEE Transactions on Wireless Communications*, vol. 19, no. 8, pp. 5218–5233, 2020.
- [38] Q. Wu, S. Zhang, B. Zheng, C. You, and R. Zhang, "Intelligent Reflecting Surface-Aided Wireless Communications: A Tutorial," *IEEE Transactions on Communications*, vol. 69, no. 5, pp. 3313–3351, 2021.
- [39] Q. Wu and R. Zhang, "Intelligent Reflecting Surface Enhanced Wireless Network via Joint Active and Passive Beamforming," *IEEE Transactions on Wireless Communications*, vol. 18, no. 11, pp. 5394–5409, 2019.
- [40] —, "Beamforming Optimization for Wireless Network Aided by Intelligent Reflecting Surface With Discrete Phase Shifts," *IEEE Transactions on Communications*, vol. 68, no. 3, pp. 1838–1851, 2020.
- [41] A. Zappone, M. Di Renzo, F. Shams, X. Qian, and M. Debbah, "Overhead-aware design of reconfigurable intelligent surfaces in smart radio environments," *IEEE Transactions on Wireless Communications*, vol. 20, no. 1, pp. 126–141, 2021.
- [42] M.-M. Zhao, Q. Wu, M.-J. Zhao, and R. Zhang, "Intelligent reflecting surface enhanced wireless networks: Two-timescale beamforming optimization," *IEEE Transactions on Wireless Communications*, vol. 20, no. 1, pp. 2–17, 2020.
- [43] A. Albanese, P. Mursia, V. Sciancalepore, and X. Costa-Pérez, "PAPIR: Practical RIS-aided Localization via Statistical User Information," in *2021 IEEE 22nd International Workshop on Signal Processing Advances in Wireless Communications (SPAWC)*, 2021, pp. 531–535.
- [44] A. Abrardo, D. Dardari, and M. Di Renzo, "Intelligent Reflecting Surfaces: Sum-Rate Optimization Based on Statistical Position Information," *IEEE Transactions on Communications*, vol. 69, no. 10, pp. 7121–7136, 2021.
- [45] C. Pan, G. Zhou, K. Zhi, S. Hong, T. Wu, Y. Pan, H. Ren, M. Di Renzo, A. L. Swindlehurst, R. Zhang *et al.*, "An overview of signal processing techniques for ris/irs-aided wireless systems," *IEEE Journal of Selected Topics in Signal Processing*, 2022.
- [46] M. E. Morochó-Cayamela, H. Lee, and W. Lim, "Machine Learning for 5G/B5G Mobile and Wireless Communications: Potential, Limitations, and Future Directions," *IEEE Access*, vol. 7, pp. 137 184–137 206, 2019.
- [47] A. Seretis and C. D. Sarris, "An Overview of Machine Learning Techniques for Radiowave Propagation Modeling," *IEEE Transactions on Antennas and Propagation*, pp. 1–1, 2021.
- [48] M. Sanchez-Fernandez, M. de Prado-Cumplido, J. Arenas-Garcia, and F. Perez-Cruz, "SVM multiregression for nonlinear channel estimation in multiple-input multiple-output systems," *IEEE Transactions on Signal Processing*, vol. 52, no. 8, pp. 2298–2307, 2004.
- [49] M. Ayadi, A. Ben Zineb, and S. Tabbane, "A UHF Path Loss Model Using Learning Machine for Heterogeneous Networks," *IEEE Transactions on Antennas and Propagation*, vol. 65, no. 7, pp. 3675–3683, 2017.
- [50] A. Alkhateeb, S. Alex, P. Varkey, Y. Li, Q. Qu, and D. Tujkovic, "Deep Learning Coordinated Beamforming for Highly-Mobile Millimeter Wave Systems," *IEEE Access*, vol. 6, pp. 37 328–37 348, 2018.
- [51] Z. Yang, Y. Liu, Y. Chen, and N. Al-Dhahir, "Machine Learning for User Partitioning and Phase Shifters Design in RIS-Aided NOMA Networks," *IEEE Transactions on Communications*, vol. 69, no. 11, pp. 7414–7428, 2021.
- [52] Y. Zhang, M. Alrabeiah, and A. Alkhateeb, "Reinforcement Learning of Beam Codebooks in Millimeter Wave and Terahertz MIMO Systems," *IEEE Transactions on Communications*, vol. 70, no. 2, pp. 904–919, 2022.
- [53] M. Tonnemacher, C. Tarver, V. Chandrasekhar, H. Chen, P. Huang, B. L. Ng, J. Charlie Zhang, J. R. Cavallaro, and J. Camp, "Opportunistic Channel Access Using Reinforcement Learning in Tiered CBRS Networks," in *2018 IEEE International Symposium on Dynamic Spectrum Access Networks (DySPAN)*, 2018, pp. 1–10.
- [54] H. Chen, X. Li, and F. Zhao, "A Reinforcement Learning-Based Sleep Scheduling Algorithm for Desired Area Coverage in Solar-Powered Wireless Sensor Networks," *IEEE Sensors Journal*, vol. 16, no. 8, pp. 2763–2774, 2016.
- [55] C. Dhahri and T. Ohtsuki, "Q-learning cell selection for femtocell networks: Single- and multi-user case," in *2012 IEEE Global Communications Conference (GLOBECOM)*, 2012, pp. 4975–4980.
- [56] X. Liu, Y. Liu, and Y. Chen, "Machine Learning Empowered Trajectory and Passive Beamforming Design in UAV-RIS Wireless Networks," *IEEE Journal on Selected Areas in Communications*, vol. 39, no. 7, pp. 2042–2055, 2021.
- [57] Y. Cheng, K. H. Li, Y. Liu, K. C. Teh, and H. V. Poor, "Downlink and uplink intelligent reflecting surface aided networks: Noma and oma," *IEEE Transactions on Wireless Communications*, vol. 20, no. 6, pp. 3988–4000, 2021.
- [58] Q. Wu, S. Zhang, B. Zheng, C. You, and R. Zhang, "Intelligent reflecting surface-aided wireless communications: A tutorial," *IEEE transactions on communications*, vol. 69, no. 5, pp. 3313–3351, 2021.
- [59] H. Lu, Y. Zeng, S. Jin, and R. Zhang, "Aerial Intelligent Reflecting Surface: Joint Placement and Passive Beamforming Design With 3D Beam Flattening," *IEEE Transactions on Wireless Communications*, vol. 20, no. 7, pp. 4128–4143, 2021.
- [60] A. Haskou and H. Khaleghi, "On the effect of ris phase quantization on communications system performances," in *2023 International Wireless Communications and Mobile Computing (IWCMC)*. IEEE, 2023, pp. 1406–1411.
- [61] C. Feng, X. Li, Y. Zhang, X. Wang, L. Chang, F. Wang, X. Zhang, and X. Chen, "Rflens: metasurface-enabled beamforming for iot communication and sensing," in *Proceedings of the 27th Annual International Conference on Mobile Computing and Networking*, 2021, pp. 587–600.
- [62] P. Mursia, V. Sciancalepore, A. Garcia-Saavedra, L. Cottatellucci, X. C. Pérez, and D. Gesbert, "RISMA: Reconfigurable Intelligent Surfaces Enabling Beamforming for IoT Massive Access," *IEEE Journal on Selected Areas in Communications*, vol. 39, no. 4, pp. 1072–1085, 2021.
- [63] M. Rossanese, P. Mursia, A. Garcia-Saavedra, V. Sciancalepore, A. Asadi, and X. Costa-Perez, "Designing, building, and characterizing RF switch-based reconfigurable intelligent surfaces," in *Proceedings of the 16th ACM Workshop on Wireless Network Testbeds, Experimental evaluation & CHaracterization*, 2022, pp. 69–76.
- [64] Freund, Roland W and Jarre, Florian, "Solving the sum-of-ratios problem by an interior-point method," *Journal of Global Optimization*, vol. 19, no. 1, pp. 83–102, 2001.
- [65] K. Shen and W. Yu, "Fractional Programming for Communication Systems—Part I: Power Control and Beamforming," *IEEE Transactions on Signal Processing*, vol. 66, no. 10, pp. 2616–2630, 2018.
- [66] S. J. Wright, *Primal-dual interior-point methods*. SIAM, 1997.
- [67] T. Zhang, R. Ramakrishnan, and M. Livny, "Birch: an efficient data clustering method for very large databases," in *SIGMOD '96*, 1996.
- [68] S. Kasdorf, B. Troksa, C. Key, J. Harmon, and B. M. Notaroš, "Advancing Accuracy of Shooting and Bouncing Rays Method for Ray-Tracing Propagation Modeling Based on Novel Approaches to Ray Cone Angle Calculation," *IEEE Transactions on Antennas and Propagation*, vol. 69, no. 8, pp. 4808–4815, 2021.
- [69] T. S. Rappaport, *Wireless Communications: Principles and Practice, Second edition*. Prentice Hall, 2001.
- [70] A. B. Sediq, R. H. Gohary, R. Schoenen, and H. Yanikomeroglu, "Optimal Tradeoff Between Sum-Rate Efficiency and Jain's Fairness Index in Resource Allocation," *IEEE Transactions on Wireless Communications*, vol. 12, no. 7, pp. 3496–3509, 2013.
- [71] F. S. Melo, "Convergence of q-learning: A simple proof," *Institute Of Systems and Robotics, Tech. Rep.*, pp. 1–4, 2001.
- [72] R. Brem and T. F. Eibert, "A Shooting and Bouncing Ray (SBR) Modeling Framework Involving Dielectrics and Perfect Conductors," *IEEE Transactions on Antennas and Propagation*, vol. 63, no. 8, pp. 3599–3609, 2015.